Title

Rice Straw Cellulose Nanofibrils via Aqueous Counter Collision and Differential Centrifugation and Their Self-Assembled Structures

Journal

ACS Sustainable Chemistry & Engineering, 4(3)

ISSN

2168-0485

Authors

Jiang, Feng
Kondo, Tetsuo
Hsieh, You-Lo

Publication Date

2016-03-07

DOI

10.1021/acssuschemeng.5b01653

Peer reviewed

ACS Sustainable Chemistry & Engineering

Research Article

pubs.acs.org/journal/ascecg

Rice Straw Cellulose Nanofibrils via Aqueous Counter Collision and Differential Centrifugation and Their Self-Assembled Structures

Feng Jiang,[†] Tetsuo Kondo,[‡] and You-Lo Hsieh*[,†]

[†]Fiber and Polymer Science, University of California at Davis, Davis, California 95616-8722, United States

[‡]Graduate School of Bioresource and Bioenvironmental Sciences, Kyushu University, 6-10-1, Hakozaki, Higashi-ku, Fukuoka 812-8581, Japan

ABSTRACT: Rice straw cellulose was completely defibrillated via aqueous counter collision (ACC) at a low energy input of 15 kWh/kg, then fractionated by differential centrifugation into four increasing weight fractions of progressively thinner cellulose nanofibrils (CNFs): 6.9% in 80−200 nm, 14.4% in 20−80 nm, 20.3% in 5−20 nm, and 58.4% in less than 5 nm thickness. The 93.1% less than 80 nm or 78.7% less than 20 nm thick CNFs yields were more than double those from wood pulp by other mechanical means but at a lower energy input. The smallest (3.7 nm thick and 5.5 nm wide) CNFs were only a third or less in lateral dimensions than those obatined through ACC processed from wood pulp, bamboo, and microbial cellulose pellicle. The less than 20 nm thick CNFs could self-assemble into continuous submicron (136 nm) wide fibers by freezing and freeze-drying or semitransparent (13−42% optical transmittance) film by ultrafiltration and air-drying with excellent mechanical properties (164 MPa tensile strength, 4 GPa Young's modulus, and 16% strain at break). ACC defibrillated CNFs retained essentially the same chemical and crystalline structures and thermal stability as the original rice straw cellulose and therefore were much more thermally stable than TEMPO oxidized CNFs and sulfuric acid hydrolyzed cellulose nanocrystals from the same rice straw cellulose.

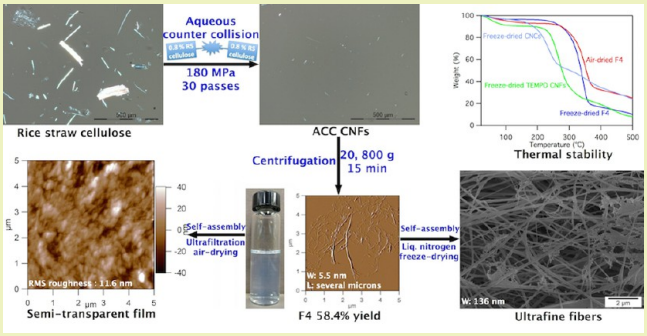

KEYWORDS: *Cellulose nanofibrils, Aqueous counter collision, Differential centrifugation, Self-assembling, Rice straw*

INTRODUCTION

Rice straw consists of similar extents of cellulose, i.e., 36.5−46.6%,[1−4] as wood and can be pulped using traditional processes,[3,5,6] extracted for long fibers by high pressure steam[7] and alkaline/enzyme[8] processes, as well as hydrolyzed into microcrystalline cellulose by hydrochloric acid[9] and enzymes.[10] Thus derived rice straw celluloses are in the form of micrometer wide or larger fibers. Although native cellulose is known to consist of a few nanometer wide elementary fibrils and tens of nanometer wide microfibrils,[11,12] mechanical defibrillation of rice straw cellulose into nanofibers was only first reported in 2009.[13] Mechanical grinding produced 12−35 nm wide nanofibrils,[13] while homogenization[14] and ultrasonication[15,16] resulted in more heterogeneous nanofibrils in 10−90 nm widths, however, without yield information.

We have derived cellulose nanocrystals (CNCs) and nanofibrils (CNFs) from rice straw cellulose via chemical means as well as in combination with mechanical shears.[17−20] Rod-like CNCs (4−7 nm thick, 110−270 nm long) were obtained by sulfuric acid hydrolysis (64 wt % H_2SO_4, 45 °C, 15−60 min) in 4.9−16.9% yields.[17−20] High-speed blending (37,000 rpm, 2 h) followed by centrifugation (1,500 rpm, 15 min) generated less than 10 nm thick and hundreds of nanometers to several micrometer long CNFs in the supernatant.[17] These CNFs were thinner than those by previously mentioned mechanical methods[13−16] but yielding only 12% from the original cellulose. Optimized 2,2,6,6-tetramethylpyperidine-1-oxyl (TEMPO) oxidation coupled with mechanical blending produced much thinner (1−3 nm wide) and longer (up to 1 μm long) CNFs at an impressive 96.8% yield.[19,21,22] These CNCs and CNFs showed intriguing self-assembling behaviors that led to ultrafine fibers[23] and amphiphilic superabsorbent aerogels.[24,25] While chemical approaches generated most homogeneous CNCs and CNFs and excellent CNF yield when combined with mechanical blending from rice straw cellulose, mechanical blending alone usually led to low yields.[17] Considering the merits of mechanical defibrillation, i.e., chemical free and greener processing, nanocellulose quality and yield of nanocellulsoe as well as energy required are among the issues that remain to be resolved.

In this study, defibrillation of rice straw cellulose was extended to include a scalable mechanical process, i.e., aqueous counter collision (ACC). In ACC, two jets of aqueous cellulose suspension collide with each other nearly head on (in 170°) at high speeds generated by high pressures in the 50−270 MPa range to pulverize micrometer wide fibers to nanometer wide

Received: December 7, 2015
Revised: January 13, 2016
Published: January 17, 2016

DOI: 10.1021/acssuschemeng.5b01653
ACS Sustainable Chem. Eng. 2016, 4, 1697−1706

fibrils at a total energy input as low as 15 kWh/kg or MWh/t.[26−28] ACC has been applied to an Iα microbial cellulose pellicle[27] and Iβ microcrystalline cellulose,[28] generating CNFs with, respectively, 34 and 15 nm widths, 3.8 and 0.92 μm lengths, and 61 and 111 aspect ratios after 60 passes. In defibrillating rice straw cellulose with ACC, the processed aqueous suspension was fractionated to four populations by differential centrifugation to fully recover all defibrillated CNFs. The geometries and morphologies of CNFs generated by ACC, as well as their assembled structures, were investigated and compared with CNCs and CNFs generated via other chemical and mechanical means from the same rice straw cellulose as well as with CNFs defibrillated from other sources via the same ACC process.

EXPERIMENTAL SECTION

Materials. Pure cellulose was isolated from rice straw (Calrose variety) by a three-step process of 2:1 v/v toluene/ethanol extraction, acidified $NaClO_2$ dissolution of lignin (1.4%, 70 °C, 5 h), and alkaline dissolution of hemicellulose and silica (5% KOH, 90 °C for 2 h) to a 36% yield.[18]

Aqueous Counter Collision (ACC) Defibrillation.[26−28] Pure rice straw cellulose was defibrillated using an aqueous counter collision (ACC) system (CNNT Co. Ltd., South Korea). An aqueous 0.8 wt % cellulose microfiber suspension was expelled through two 160 μm diameter nozzles at 180 MPa pressure, whereupon two streams collided at 170° (5° deviation from head-on collision), rapidly wet pulverizing into aqueous dispersion of defibrillated cellulose. The ACC process was repeated for a total of 30 pulverizing cycles or passes at a total 15 kWh/kg or MWh/t energy input for 30 ACC passes.

Fractionation of Cellulose Nanofibrils (CNFs) via Differential Centrifugation. The ACC processed suspension was fractionated by differential centrifugation at three increasing angular velocities of 1,500, 5,000, and 14,000 rpm for 15 min, and the three precipitated fractions were designated as F1, F2, and F3, respectively, with the fraction in the final supernatant denoted as F4. The relative centrifugal forces (RCF) calculated from the three angular velocities (ω) and radius of centrifuge (r),[29] were 405, 4,500, and 20,800g, respectively.

$$\mathrm{RCF} = 1.118 \times 10^{-6}\omega^2 r \tag{1}$$

A few milliliters of each fraction were oven-dried and weighed to determine its weight percentage and to calculate the yield of each based on the original pure cellulose.

During centrifugation, CNFs experience a driving centrifugal force (F) as well as two counter buoyant force (F_b) and frictional force (F_f) that prevent the fibers from moving away from the center of the centrifuge.[29]

$$F = \rho_c V\omega^2 r \tag{2}$$

$$F_b = \rho_w V\omega^2 r \tag{3}$$

$$F_f = f_v \tag{4}$$

where V is the volume of the CNFs; ρ_c and ρ_w are densities of CNF (1.6 g/cm^3) and water (1 g/cm^3), respectively; f is the frictional coefficient, and v is the rate of sedimentation. Assuming CNFs conform into spherical particles with a hydrodynamic radius (r_h) determined from dynamic light scattering (Table 1), V could be expressed as

$$V = \frac{4}{3}\pi r_h^3 \tag{5}$$

and f could be expressed by Stokes equation as

$$f = 6\pi\eta r_h \tag{6}$$

where η is the viscosity of water: 0.894 mPa·s.

The CNFs start to precipitate at v when all forces are at balance

$$F = \frac{4}{3}\pi r_h^3\rho_c\omega^2 r = F_b + F_f = \frac{4}{3}\pi r_h^3\rho_w\omega^2 r + 6\pi\eta r_h v \tag{7}$$

Therefore, the rate of sedimentation v could be expressed as

$$v = \frac{2r_h^2(\rho_c - \rho_w)\mathrm{RCF}}{9 \times 1.118 \times 10^{-6}\pi} \tag{8}$$

The sedimentation coefficient s (unit S, Svedberg, 1 S = 10^{-13} s) could be expressed

$$S = \frac{v}{\omega^2 r} = \frac{2r_h^2(\rho_c - \rho_w)}{9\eta} \tag{9}$$

It should be noted that CNFs are in nanofibrillar form and that the hydrodynamic radius obtained from dynamic light scattering (DLS) is approximately the radius of a hypothetical sphere of the randomly coiled CNFs with the same translational diffusion coefficient[30] but did not represent the actual fibrillar dimensions. Therefore, both the rate of sedimentation and sedimentation coefficient derived therefrom should also be taken as relative values to be compared only across the different fractions.

Characterization of Aqueous Suspensions. The optical transmittance of 0.1 wt % F1−F4 suspensions was recorded from 300 to 800 nm using an Evolution 600 UV−vis spectrophotometer (Thermo Scientific) in a quartz cuvette. Pure cellulose before and after ACC treatment at 0.1 wt % was placed between a glass slide and coverslip and observed under a Leica DM2500 optical microscope equipped with a cross-polarized filter. DLS experiments were performed on 0.05% F1−F4 at 25 °C with a Zetasizer Nano S90 (Malvern Instrument, Ltd.) at a detection angle of 90°, without adding salt to adjust the ionic strength. Reported values are z-average radius (averaged from triplicate measurements) obtained with the General Purpose algorithm of the Zetasizer Nano software. All F1−F4 suspensions (10 μL, 0.002 wt %) were deposited onto a freshly cleaved mica surface, air-dried, and scanned using an OMCL-AC160TS standard silicon probe in tapping mode on an atomic force microscope (Asylum-Research MFP-3D) under ambient conditions at 1 Hz scan rate and 512 × 512 pixels image resolution. The height of images and profiles were processed with Igor Pro 6.21 loaded with MFP3D 090909 + 1409, and the average thickness was determined from ca. 200 individual CNFs. F4 suspension (8 μL, 0.01 wt %) was deposited onto glow-discharged carbon-coated TEM grids (300-mesh copper, Formvar-carbon, Ted Pella Inc., Redding, CA) with the excess liquid removed by blotting with a filter paper after 10 min. The specimen was then negatively stained with 2% uranyl acetate solution for 5 min, blotted with a filter paper to remove excess liquid, and allowed to dry under ambient conditions, and then observed using a Philip CM12 transmission electron microscope operated at a 100 kV accelerating voltage. The width was measured from ca. 200 individual nanofibrils using an image analyzer (ImageJ, NIH, USA).

Characterization of Self-Assembled CNFs. Aqueous suspensions (20 mL) of the four fractions (F1−F4) at 0.1 wt % were rapidly frozen in liquid nitrogen and lyophilized at −50 °C in a freeze-drier (FreeZone 1.0L Benchtop Freeze-Dry System, Labconco, Kansas City, MO) into a fibrous mass.

XRD spectra for pure cellulose and self-assembled F1−F4 were collected on a Scintag XDS 2000 powder diffractometer using a Ni-filtered Cu Kα radiation (λ = 1.5406 Å) at an anode voltage of 45 kV and a current of 40 mA. Solid samples were compressed between two glass slides into flat sheets with around 1 mm thickness. Diffractograms were recorded from 5° to 40° at a scan rate of 2°/min. Crystallinity index (CrI) was calculated from the intensity of the 200 peak (I_{200}, 2θ = 22.6°) and the intensity minimum between the peaks at 200 and 110 (I_{am}, 2θ = 18.7°) by using the empirical equation[31]

$$CrI = \frac{I_{200} - I_{am}}{I_{200}} \times 100 \tag{10}$$

The crystallite dimensions of these samples were calculated using Scherrer equation:[32]

DOI: 10.1021/acssuschemeng.5b01653
ACS Sustainable Chem. Eng. 2016, 4, 1697−1706

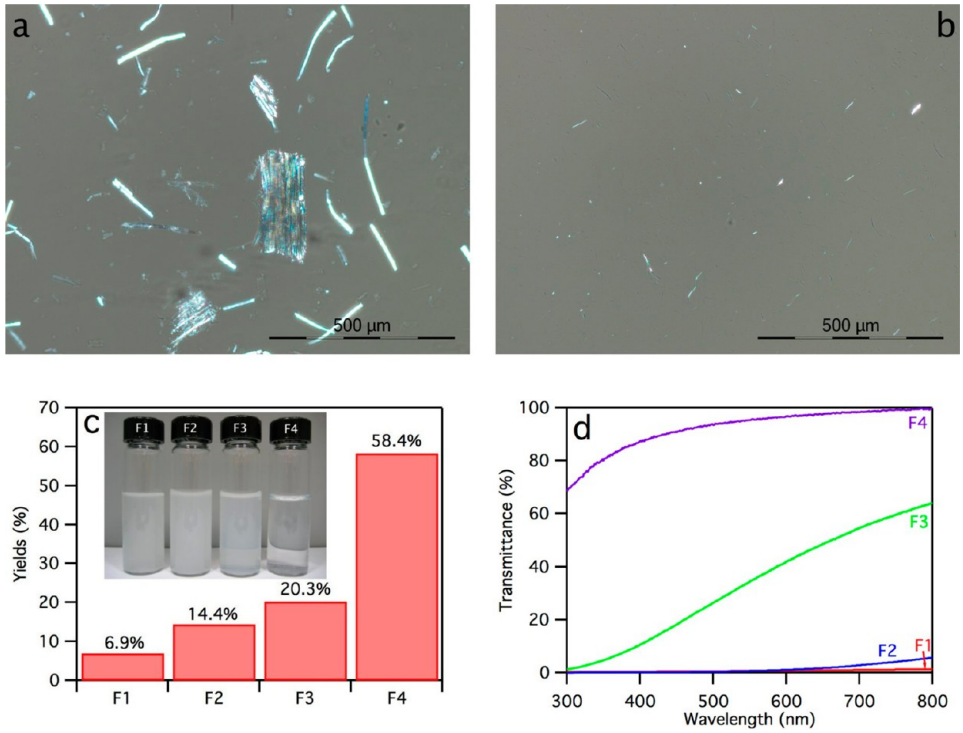

Figure 1. Optical microscopic images of rice straw cellulose under a cross-polarizer before (a) and after (b) ACC treatment; yields (c) and transmittance (d) of aqueous suspensions of F1−F4. The insets in c are photographs of F1−F4 at 0.1%.

$$D_{hkl} = \frac{0.9\lambda}{\beta_{1/2}\cos\theta} \quad (11)$$

where D_{hkl} is the crystallite dimension in the direction normal to the *hkl* lattice planes, λ is the X-ray radiation wavelength (1.5406 Å), $\beta_{1/2}$ is the full width at half-maximum of the diffraction peak, and θ is the corresponding Bragg angle. $\beta_{1/2}$ was determined from Voigt profile fits of the diffraction peaks calculated with PeakFit (v4.12, Systat Software, Inc.).

FTIR spectra of freeze-dried pure cellulose and F1−F4 in KBr pellets (1:100, w/w) were collected using a Thermo Nicolet 6700 spectrometer. The spectra were collected at ambient conditions in the transmittance mode from an accumulation of 128 scans at a 2 cm^{-1} resolution over the regions of 4000−400 cm^{-1}. TGA analyses of pure cellulose and F1−F4 were performed on a TGA-50 thermogravimetric analyzer (Shimadzu, Japan). Each sample (3−4 mg) was heated at 10 °C/min from 25 to 500 °C under purging N_2 (50 mL/min). Freeze-dried F1−F4 were mounted with conductive carbon tape, sputter coated with gold, and imaged by a field emission scanning electron microscope (FE-SEM) (XL 30-SFEG, FEI/Philips, USA) at a 5 mm working distance and 5 kV accelerating voltage. The diameters of freeze-dried CNFs were calculated from measurements of over 100 individual fibers using an image analyzer (ImageJ, NIH, USA).

Characterization of Vacuum-Filtered CNF Films. Aqueous suspensions (60 mL, 0.1%) containing F4 and combined F3 and F4 were filtered through a nylon membrane (200 nm pore size, Millipore, Billerica, MA) and allowed to air-dry under ambient conditions, then rewetted to be detached and further dried in between two membranes at room temperature. The densities of both films were determined from the weight and dimensions of films in triplicates, weighing with a precision balance (0.1 mg resolution, Sartorius, Germany) and measuring with a caliper (0.01 mm resolution, Neiko 01407A, Neiko Tools, USA) for length and width and a micrometer (1 μm resolution, Mitutoyo No. 293-340, Japan) for thickness. The optical transmittance of films was recorded from 350 to 800 nm using an Evolution 600 UV−vis spectrophotometer. The surface morphologies were scanned using an atomic force microscope as previously described, and the root square mean (RSM) roughness was calculated based on scanning over a 5 μm × 5 μm area on the height images using MFP3D 090909 + 1409 plugin in IGOR Pro 6.21. Both TGA and XRD of CNF films were analyzed as previously stated for the freeze-dried samples.

The tensile properties of the CNF films were measured on an Instron tensile tester (model 5566) fitted with a pair of pneumatic grips. The films with a typical thickness of 40 μm were cut into 4 mm wide and 30 mm long specimens, and each film was tested in triplicate at a 10 mm gauge length and a constant 1 mm/min strain rate until breakpoint at 23 °C and 60% humidity. Young's modulus defined by the initial slope of the $\sigma-\varepsilon$ curve as well as the ultimate tensile stress (σ) and strain at break (ε) were averaged, and the mean and standard deviation values were reported.

RESULTS AND DISCUSSION

ACC Treated Rice Straw Cellulose. Pure cellulose was isolated from rice straw by extraction with toluene/ethanol, delignification with acidified sodium chlorite, and bleaching with potassium hydroxide[18] to be in the forms of 5−10 μm wide and 50−300 μm long microfibers and few thin sheets of parallel microfibers, all brightly birefringent under the cross-polarizer, indicative of their highly crystalline nature (Figure 1a). After 30 ACC passes, only a few of the smallest microfibers remained visible at the same concentration, indicating that most of the original microfibers were significantly defibrillated into dimensions less than the visible light wavelengths (Figure 1b).

The ACC processed aqueous suspension was centrifuged at increasing centrifugal forces of 405, 4,500, and 20,800*g* and the precipitates collected as F1, F2, and F3 fractions at 6.9, 14.4, and 20.3%, respectively, leaving 58.4% F4 in the final supernatant (Figure 1c). The resuspended F1 and F2 appeared turbid and opaque, transmitting nearly nothing in most of the visible light range and only 1.4 and 5.7% at 800 nm, respectively (Figure 1c and d), indicating the CNF to be larger than the visible light wavelengths of 400 to 800 nm. The F3 suspension transmitted 10.6 to 64.1% visible light, suggesting dimensions

DOI: 10.1021/acssuschemeng.5b01653
ACS Sustainable Chem. Eng. 2016, 4, 1697−1706

to be comparable to the visible light wavelengths, while the F4 suspension appeared mostly transparent, transmitting 87.4 to 99.6% visible light.

The hydrodynamic radii of CNFs in aqueous suspensions were measured by DLS to give apparent sizes of 1,066, 652, 332, and 143 nm (Table 1) for F1, F2, F3, and F4, respectively,

Table 1. Hydrodynamic Radii, Sedimentation Parameters, and Yields of Each CNF Fraction

samples	F1	F2	F3	F4
angular velocity (ω, rpm)	1,500	5,000	14,000	NA
RCF (g)	405	4,500	20,800	NA
hydrodynamic radius (r_h, nm)	1066 ± 51	652 ± 99	332 ± 11	143 ± 6
sedimentation coefficient (S)	1.7×10^6	6.3×10^5	1.6×10^5	3.0×10^4
yield (%)	6.9	14.4	20.3	58.4

consistent with decreasing dimensions of CNFs fractionated at increasing centrifugal forces. These hydrodynamic dimensions were consistent with the light transmission data where the CNFs in F1 and F2 exceeded and those in F3 and F4 were largely less than the visible light wavelengths. Clearly, CNFs derived via 30 ACC passes were heterogeneous in size, and the different size populations could be easily fractionated by varying centrifugal forces.

The CNFs remained in the supernatant at 4,500*g* centrifugal force, i.e., F3 and F4 combined, was 78.7%. This CNF yield is even higher than that of other mechanically defibrillated CNFs that were fractionated at lower centrifugal forces, i.e., 53% Avicel CNFs from high-intensity ultrasonication for 60 min (centrifuged at 900*g*)[33] and 40% bleached eucalyptus kraft pulp CNFs from grinding with an energy input of 40 kWh/kg (centrifuged at 200*g*).[34] The 58.4% yield of the finest F4 CNFs in the last supernatant (centrifuged at 20,800*g*) was nearly double that from the microfluidizer treated softwood kraft pulp (29.4% centrifuged at 10,000*g*)[35] while with only one-fourth of the energy input (15 vs 55.3 MWh/t) or 1.5 times of that from grinding eucalyptus kraft pulp[33] and also with only one-third of energy consumption (15 vs 40 kWh/kg). The lower energy required to defibrillate rice straw cellulose by ACC and the high CNF yields clearly demonstrate ACC to be a more energy-efficient way to generate cellulose nanofibrils from rice straw than other mechanical means from wood pulp.

Comparing the different defibrillations of the same rice straw cellulose, 2-h high speed blending alone yielded only 12% CNFs[14] far lower than the 93.1% CNFs from ACC (both centrifuged at 405*g*).[14] In coupling TEMPO oxidation with high speed blending (30 min) of rice straw cellulose, 42.7, 80.7 and 96.8% CNFs were produced (centrifuged at 4,500*g*) with increasing oxidization at 1.5, 3, and 5 mmol primary oxidant NaClO per g of cellulose.[21] The cumulative 78.7% yield of ACC-processed CNFs fractionated at the same 4,500*g* is comparable to that (80.7%) from coupled moderate oxidation and 30-min blending, clear evidence of similar effectiveness of ACC as a chemical free means to defibrillate rice straw cellulose.

As all aqueous CNF suspensions have the same cellulose densities and solution viscosities, the sedimentation coefficient should be only proportional to the square root of the hydrodynamic radius as shown in eq 9. The 2 orders of

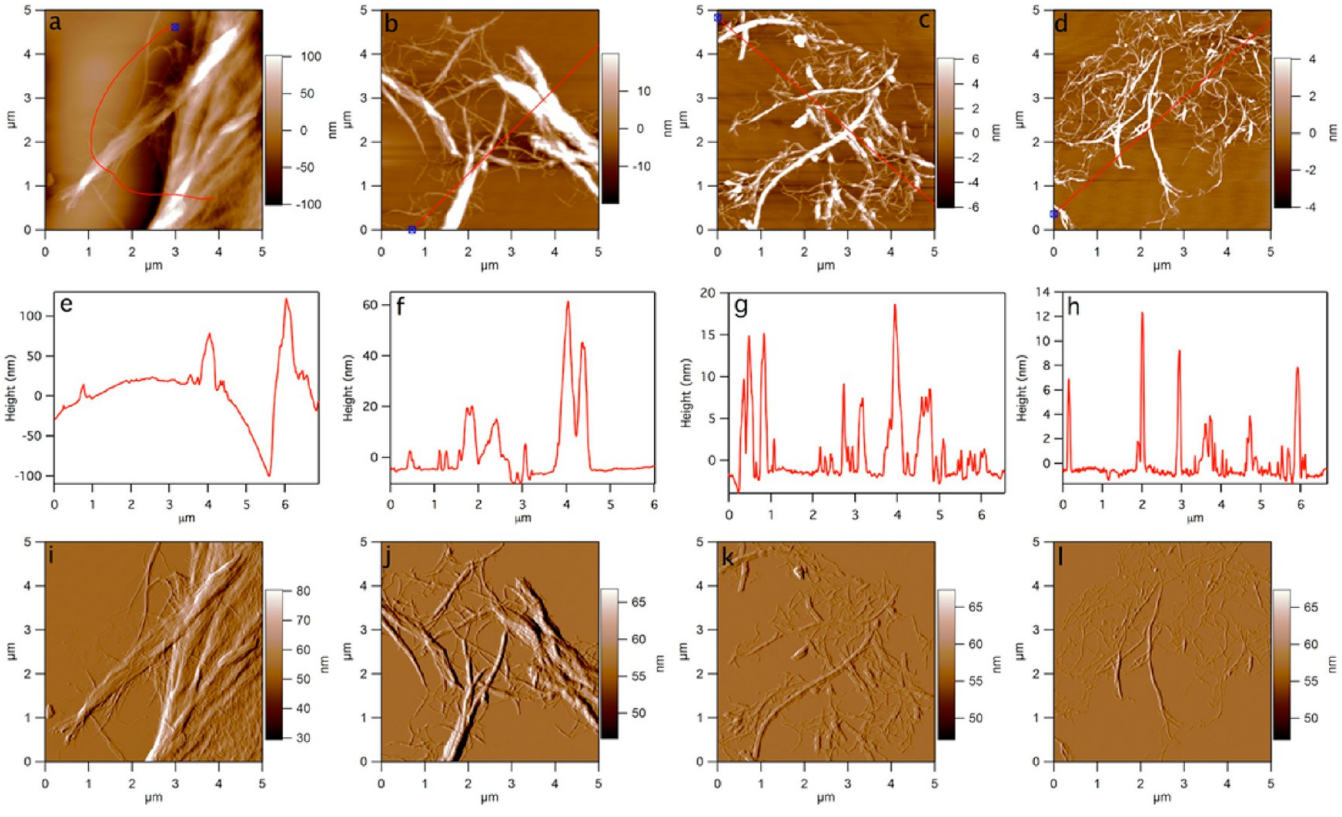

Figure 2. AFM height images (a–d), height profiles (e–h), and phase images (i–l) of ACC treated rice straw cellulose F1 (a,e,i), F2 (b,f,j), F3 (c,g,k), and F4 (d,h,l).

DOI: 10.1021/acssuschemeng.5b01653
ACS Sustainable Chem. Eng. 2016, 4, 1697–1706

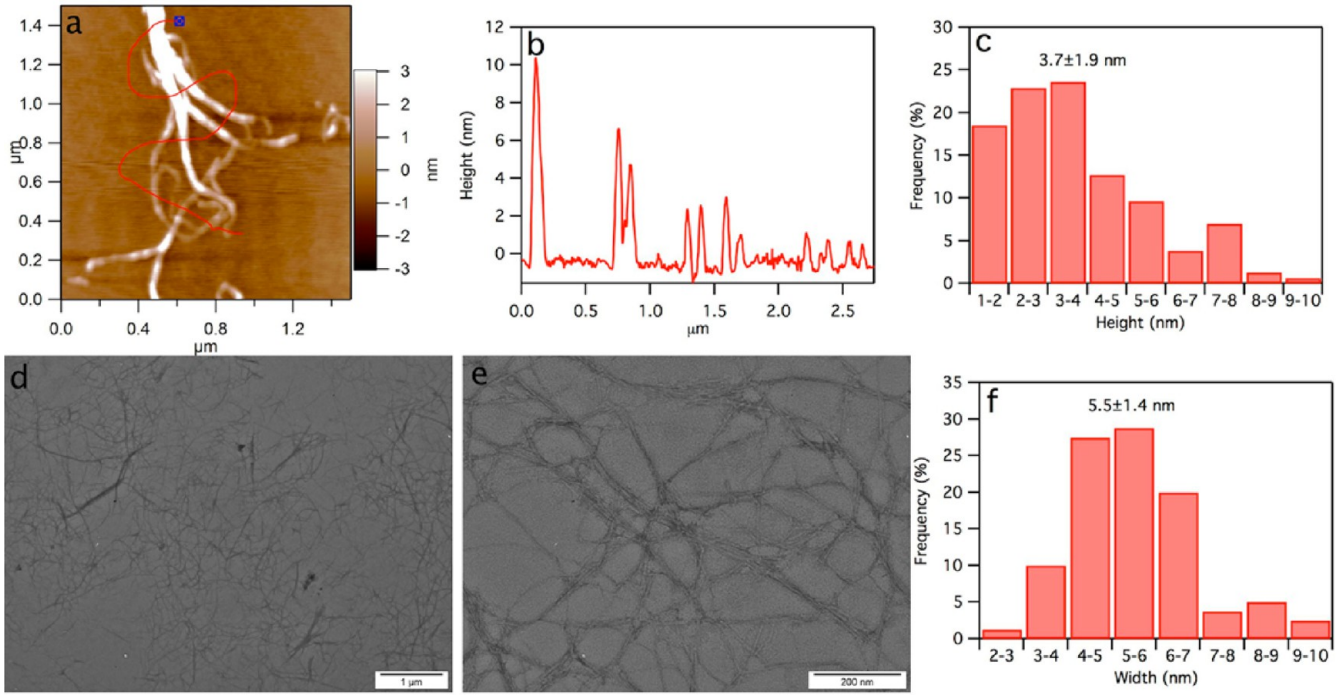

Figure 3. AFM height image (a), height profile (b), distribution (c) TEM images (d,e), and width distribution (f) of ACC treated F4 cellulose nanofibrils.

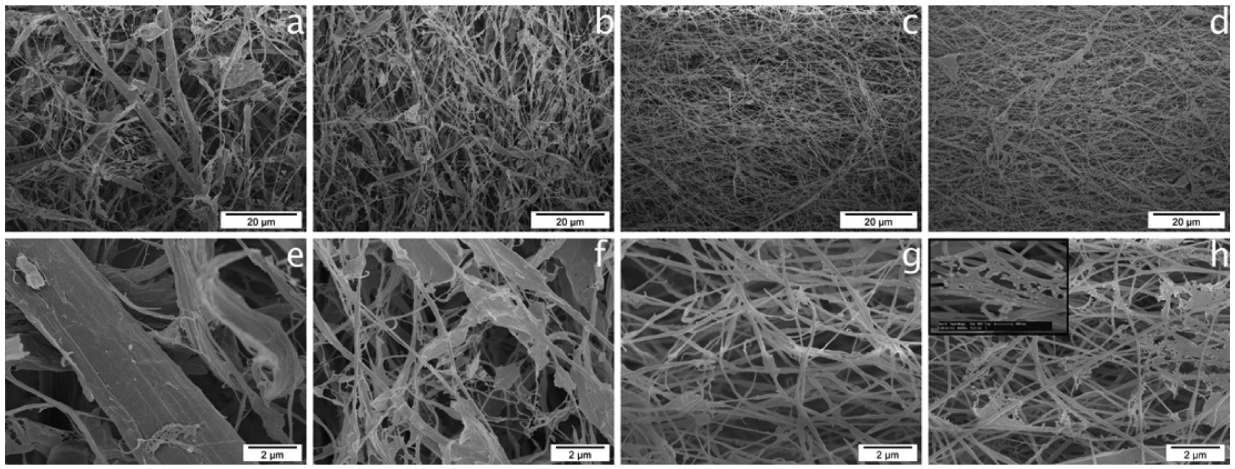

Figure 4. SEM images of self-assembled CNFs. (a,e) F1; (b,f) F2; (c,g) F3; (d,h) F4.

magnitude decrease in the sedimentation coefficient and distinctly different hydrodynamic radius among these fractions confirmed the effectiveness of differential centrifugation in fractionating ACC processed CNFs. Again, considering the assumption made on the hydrodynamic radius, only a relative comparison of the sedimentation coefficient should be made out of this.

Visualization of CNFs in the four fractions by AFM and TEM showed F1 to consist of larger frayed fibers approaching ca. 200 nm in height and partially liberated and protruding nanofibrils in ca. 80 nm height (Figure 2a,e,i). The large fiber sizes observed corresponded well with the low transmittance and large hydrodynamic radius of F1. A similarly defibrillated structure was observed in F2, but the CNFs were less than 60 nm and most prevalent ca. 20 nm in height (Figure 2b,f,j). F3 contained mainly ca. 20 nm and some 5 nm nanofibrils (Figure 2c,g,k), whereas nanofibrils in F4 were primarily less than 5 nm in height, with few over 15 nm (Figure 2d,h,l). Therefore, ACC processed rice straw cellulose suspension could be separated by increasing RCF into thinner CNFs in increasing weight fractions: 6.9% 80−200 nm, 14.4% 20−80 nm, 20.3% 5−20 nm, and 58.4% less than 5 nm.

Further visualization of F4 CNFs by AFM at a higher magnification clearly showed the fraying of a 11 nm nanofibril into two 5−7 nm nanofibrils, each fraying into several 2−3 nm nanofibrils and finally to 1 nm nanofibrils, with an overall average thickness of 3.7 ± 1.9 nm (Figure 3a−c). TEM showed similarly branched fibrils with progressively narrower CNFs as observed under AFM, with 5.5 ± 1.4 nm averaged width and several micrometer lengths (Figure 3d−f). In essence, the ACC defibrillated nanofibrils are mostly branched, in contrast to the individual CNFs from TEMPO oxidation.[21] Similarly branched nanofibrils have also been observed from high-speed blending,[17] indicating that cellulose nanofibrils could not be

DOI: 10.1021/acssuschemeng.5b01653
ACS Sustainable Chem. Eng. 2016, 4, 1697−1706

completely separated by mechanical forces alone, leaving the nanofibrils interconnected with each other in branched structures.

While CNFs from both ACC and coupled TEMPO-blending have similar ca. 1.5 aspect ratios in their cross-sectional dimensions, ACC defibrillated CNFs were about 2.5 times larger in their lateral dimensions (3.7 nm thick, 5.5 nm wide) than those of the TEMPO oxidized (1.5 nm thick, 2.1 nm wide) ones as well as being several times longer, manifesting less extensive defibrillation in both lateral and longitudinal directions of the cellulose fibers by ACC mechanical means alone. In comparison to ACC generated CNFs from various sources, the 3.7 nm thick and 5.5 nm wide rice straw CNFs are clearly smaller than those for bamboo (20.4 nm) and hardwood kraft pulp (20.8 nm),[36] microbial cellulose pellicle (33 nm),[27] and microcrystalline cellulose (17 nm).[28] The much smaller lateral dimensions of ACC treated rice straw CNFs could be due to its smaller crystallite dimension (3.5 nm)[17] as well as the less tenacious hydrogen bonding among the crystalline domains in rice straw cellulose.

Rapid freezing 0.1 wt % aqueous ACC processed suspensions in liquid nitrogen and lyophilizing at −50 °C caused CNFs to self-assemble into a fluffy fibrous mass containing submicrometer to micrometer wide and over one hundred micrometer long fibers in all cases (Figure 4 and Table 2). Self-assembled fibers from F1 were 338 ± 187 nm wide, among some undefibrillated original microfibers. Much finer 189 ± 73 nm wide fibers along with micrometer wide films were observed from F2, whereas similarly uniform and finer submicron fibers were assembled from both F3 (137 ± 44 nm wide) and F4 (136 ± 44 nm wide). In addition, some even finer 27.1 ± 7.3 nm wide nanofibers were assembled from F4. Overall, finer CNFs tend to assemble into smaller and more uniform submicron sized fibers. In fact, the finest (<20 nm) and highest proportion (78.7%) of CNFs from F3 and F4 assembled into the most uniform submicron fibers in ca. 140 nm widths. Besides extensive lateral assembling, massive assembly in the longitudinal direction was also apparent in all CNF fractions as indicated by their over 100 μm lengths.

Table 2. Morphologies and Fiber Diameters of Self-Assembled ACC Processed CNFs

samples	assembled morphologies	submicron fiber diameters (nm)
F1	submicron fibers; microfibers	338 ± 187
F2	submicron fibers, films	189 ± 73
F3	submicron fibers	137 ± 44
F4	submicron fibers	136 ± 44
	nanofibers aggregates, films	27.1 ± 7.3

The fibers assembled from F3 and F4 are much smaller (136−137 nm) than those from sulfuric acid hydrolyzed CNCs (440−511 nm wide)[17,23] and highly charged TEMPO oxidized CNFs (500 nm to a few microns wide)[21,23] under the same freeze-drying process, suggesting a lower assembling tendency of these noncharged CNFs. In fact, the self-assembled fibers from F3 and F4 have diameters close to those from high-speed blended CNFs (153 nm) and TEMPO oxidized CNFs with a low surface charge density of 0.59 mmol/g (125 nm), all CNFs having similar lateral dimensions ranging from 2 to 12 nm.[17,21] In contrast, more extensive lateral assembly seems to be favored by either a small aspect ratio in CNCs or more hydrogen bonding capacity in the highly carboxylated CNFs. Uncharged CNFs defibrillated by mechanical means, such as mechanical blending and ACC reported here, or minimal charged TEMPO oxidized CNFs tend to assemble into much finer (<200 nm wide) and uniformly sized fibers. The lower assembling behaviors of mechanically treated CNFs may be attributed to their much lower specific surfaces and hydrogen bonding capabilities as a result of their larger dimensions and branched structures.

The self-assembled fibers from all four fractions showed similar X-ray diffraction (XRD) patterns as pure rice straw cellulose, i.e., cellulose Iβ characteristic peaks at 2θ = 14.7, 16.8, and 22.7° (Figure 5a), representing the $1\bar{1}0$, 110, and 200 crystallographic planes of the monoclinic lattice structure, respectively. Although pure cellulose showed a small peak at 2θ of 34.5°, a reflection of the 004 plane of the periodic structure of the crystallite along the axial direction,[37] the peak disappeared in all four fractions. The loss of 004 peaks did not indicate the crystal structure change, as this peak is sensitive to the twisting and alignment of microfibrils and even the moisture content.[38,39] All four had similar crystallinity index (CrI) values between 77 and 79%, higher than 72.2% of the

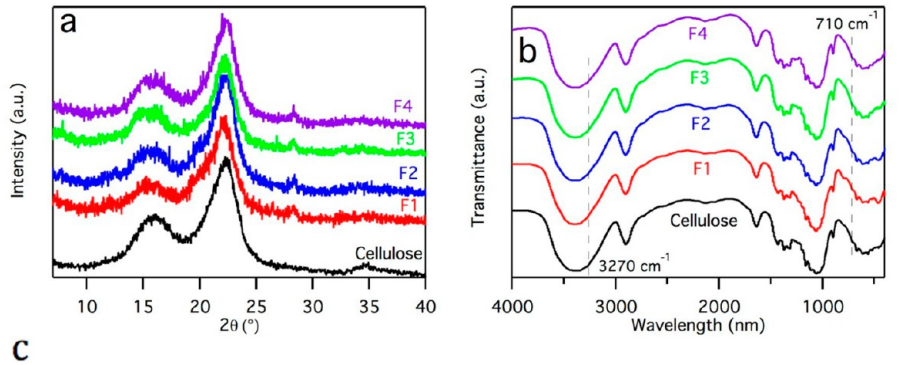

c

Samples	Cellulose	F1	F2	F3	F4
CrI (%)	72.2	77.5	77.2	78.9	77.9
D_{hkl} (nm)	3.51	3.43	3.67	3.60	3.49

Figure 5. X-ray diffraction (a), FTIR (b), and crystallinity and crystallite size (c) of rice straw α-cellulose and CNFs.

DOI: 10.1021/acssuschemeng.5b01653
ACS Sustainable Chem. Eng. 2016, 4, 1697−1706

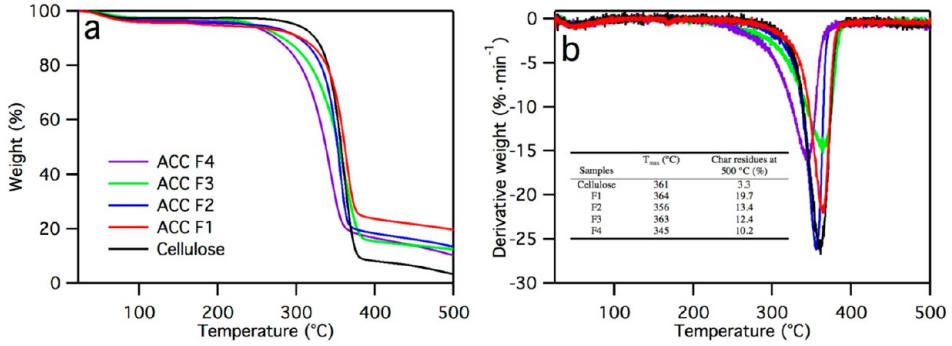

Figure 6. TGA and DTGA of rice straw α-cellulose and ACC treated CNFs.

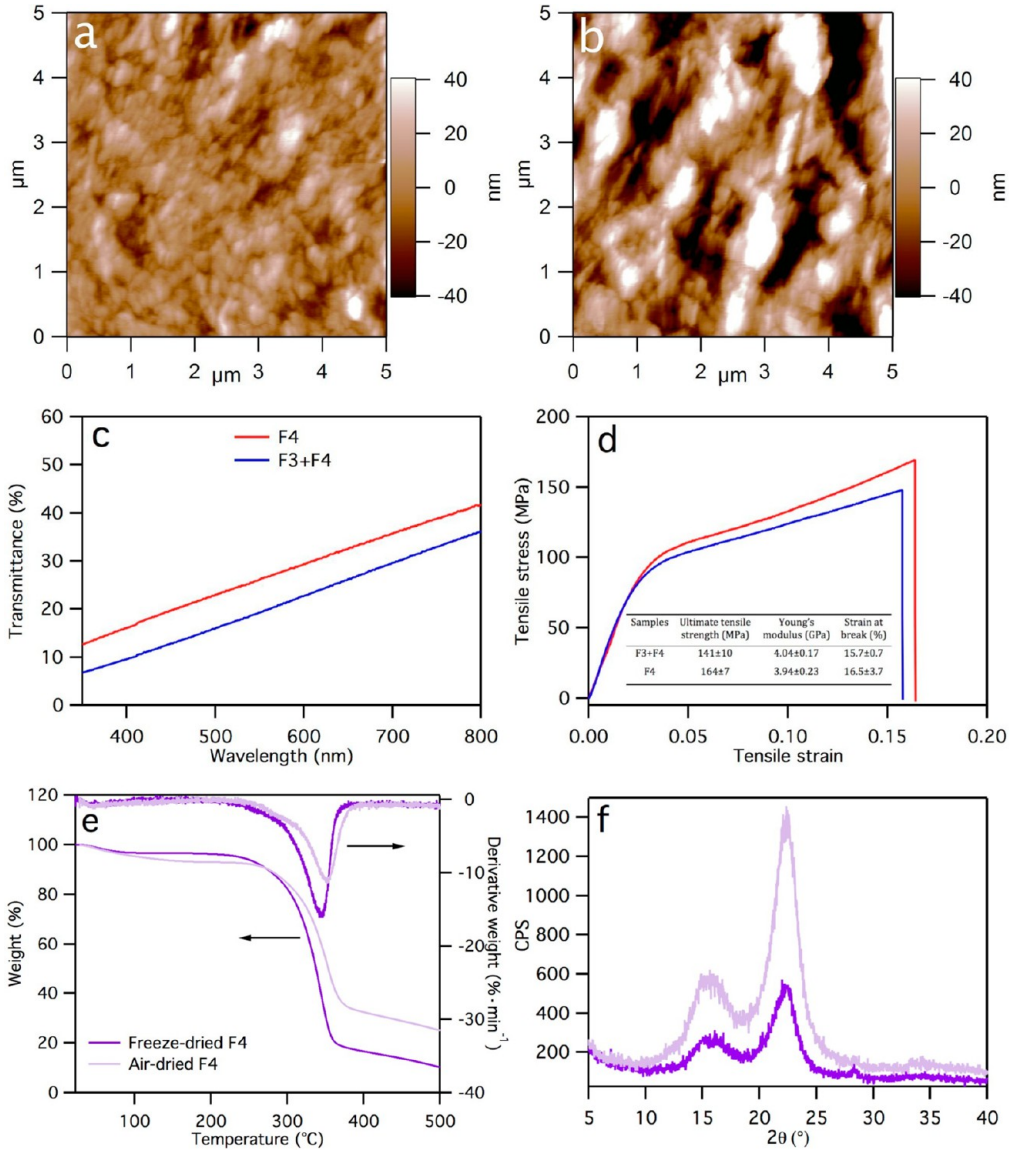

Figure 7. AFM height images (a,b), UV−vis transmittance (c), and tensile stress−stain curves (d) of F4 (a) and F3+F4 (b) films; TGA, DTGA (e), and X-ray diffraction (f) of freeze- and air-dried F4.

original pure rice straw cellulose and similar to the increased crystallinity (81.5%) of that assembled from uncharged CNFs derived from high speed blending of the same rice straw cellulose.[17] The increased CrI values suggest crystallization of uncharged surface chains on CNFs and/or the smallest nanofibrils during the freezing and freeze-drying process. The crystallite sizes of all four fractions fall in the 3.43−3.67 nm range, close to the 3.51 nm crystallite size for pure cellulose. The unchanged crystallite size indicates ACC primarily breaking the bonding among elementary fibrils without affecting those within the original ordered structured crystallites. This is in contrast to the reduced crystallite

DOI: 10.1021/acssuschemeng.5b01653
ACS Sustainable Chem. Eng. 2016, 4, 1697−1706

dimensions of 2.27 nm for TEMPO oxidized CNFs,[17] where the primary C6 hydroxyls within the crystallites might have been oxidized to break the interchain hydrogen bonding and aid defibrillation into the original crystallites.

The FTIR spectra of ACC treated CNFs exhibited no chemical structural change as expected and were identical to pure rice straw cellulose with characteristic cellulosic peaks, i.e., O−H, CH, and C−O stretching vibrations at 3400, 2900, and 1060 cm^{-1}, respectively, and the O−H bending vibration of absorbed water at 1640 cm^{-1} (Figure 5b). The cellulose Iβ structure was further supported by the small shoulders at 3270 and 710 cm^{-1}, characteristic of OH stretching and out-of-plane bending of cellulose Iβ, respectively.[21,40]

Rice straw cellulose and assembled F1 and F2 decomposed between 280 and 390 °C, whereas assembled F3 and F4 decomposed at slightly lowered temperatures of 240−380 °C (Figure 6). A shift to lower degradation temperatures from F1 to F4 was observed in the TGA curves, indicating a possible correlation to the decreasing fiber diameters or increased specific surface effects to heat. The degradation temperatures at maximum weight loss rate (T_{max}) were observed at 361, 364, 356, 363, and 345 °C for rice straw cellulose and assembled F1, F2, F3, and F4, respectively, showing a slightly lower degradation temperature for F4 only, possibly due to the much narrower 27 nm wide nanofibers, not observed in others. Nevertheless, even the most reduced T_{max} for F4 (345 °C) is much superior than those of chemically derived nanocellulose, i.e., CNCs from sulfuric acid hydrolysis (234 °C) and CNFs from TEMPO oxidation (269 °C), and slightly higher than that from mechanical blending (320 °C).[17,21] The higher thermal stability of ACC defibrillated CNFs could be ascribed to their larger dimensions and the absence of surface chemical alternation, whereas both sulfates in CNCs and carboxyls in TEMPO oxidized CNFs have shown to lower the activation energy of decomposition.[17,21] While neutralization of acid sulfate groups on CNCs and subsequent dialysis have shown to increase the T_{max} to over 300 °C,[41,42] this approach required yet additional steps for the chemical defibrillation processes.

Assembled F1, F2, F3, and F4 also showed much higher char residues of 19.7, 13.4, 12.4 and 10.2%, respectively, three to six times higher than that from the original rice straw cellulose (3.3%). The char residues for the finest F4 are lower than those from sulfuric acid hydrolyzed CNCs (23.9%), mechanically blended CNFs (20.3%), TEMPO oxidized CNFs (16.9%),[17] and TEMPO oxidized and mechanical blended CNFs (19.0%).[21] Lower char residue of ACC processed CNFs than CNCs and TEMPO oxidized CNFs is expected, considering the lack of surface sulfate and carboxyl groups, both of which replace hydroxyls to reduce cellulose depolymerization through intramolecular transglycosylation.[21,43] In conclusion, the assembled ACC treated CNFs decomposed at similar or slightly lower temperatures than the original cellulose and thus are much more thermally stable than other types of nanocellulose derived from the same source.

The largest single fraction F4 (58.4%) and the combined F3+F4 fraction (78.7%) were also fabricated into semi-transparent 40−44 μm thick films by ultrafiltration and air-drying, with respective densities of 1.377 ± 0.023 and 1.374 ± 0.045 g/cm^3. Both film surfaces showed elongated bulges resembling the overlapped aggregated cellulose nanofibrils but without any individual CNFs (Figure 7a,b). The F3+F4 film surface showed significantly larger bulges as well as deep grooves, consistent with the higher roughness. The F4 film was smoother with a root-mean-square (RMS) roughness of 11.6 nm as compared to the more than doubled 27.9 nm RMS roughness of the F3+F4 film observed from AFM height images. The F4 and F3+F4 films transmit only 13−42 and 7−36% in the 350−800 nm wavelength range, respectively (Figure 7c), significantly lower than the 80−100% transmittance of their aqueous suspensions (Figure 1d), corroborating the extensive aggregations as observed from the AFM images. The optical transmittance of these ACC CNF films are similar to those prepared from TEMPO oxidized CNFs with all protonated carboxylic acid surfaces (9−38%) but much lower than those with highly charged sodium carboxylate surfaces (30−81%).[44] We have previously shown that the higher hydrogen bonding capacity of the carboxylic acid groups on TEMPO oxidized CNFs tend to induce more aggregation, leading to reduced light transmittance. Although bearing no carboxylic acid groups, the ACC treated CNFs are branched, thicker, and longer than the TEMPO oxidized CNFs, which could explain the more aggregated morphology likely due to stiffer and more entangled CNFs.

F4 and F3+F4 films showed similar Young's modulus values of 3.94 and 4.04 GPa and strain at a break of 16.5 and 15.7%, respectively, but F4 films had approximately 16% higher ultimate tensile stress (164 MPa) than F3+F4 films (141 MPa) (Figure 7d). The higher breaking stress for F4 film could be attributed to the smaller and more uniform CNF lateral dimensions and more uniform film morphology as opposed to the heterogeneous F3+F4 film with internal and surface irregularities, consistent with an earlier report that larger fibrils could lead to more intrinsic defects to lower the mechanical properties.[45]

The rice straw CNF films showed tensile strength similar to that of ACC CNF from hardwood and bamboo (164 and 151 MPs, respectively) but more than double the strain at break (6.9 and 5.6%, respectively) and a slightly lower Young's modulus (6.9 and 6.7 GPa, respectively).[36] The differences in mechanical properties could be attributed to both sources, morphological differences among these CNFs, as well as film preparation. Both the ultimate tensile strength and Young's modulus of these films from ACC processed rice straw CNFs are lower than those (208−275 MPa tensile strength; 6.2−9.8 GPa Young's modulus) of TEMPO processed wood pulp CNF films[45−47] but showed almost double the strain at break. The decreased tensile strength and Young's modulus could be due to the larger and more heterogeneous dimensions of ACC CNFs, whereas their greater lengths could contribute to the higher strain by more entanglement to reduce slippage.

Thermal stability and crystal structure of both freeze- and air-dried F4 were showed in Figure 7e and f to examine the effect of drying. Air-dried film from F4 showed a degradation temperature at maximum weight loss rate (T_{max}) of 353 °C and 25.1% char residues at 500 °C, much higher than the respective 345 °C and 10.2% of its freeze-dried fibrous counterpart. The low thermal stability of freeze-dried CNF could be due to its higher specific surface and much shorter heat diffusion path of the ultrathin fibers, consistent with our previous observation with the TEMPO oxidized CNFs.[44] The XRD spectra of air-dried F4 showed cellulose Iβ lattice structure similar to that of the freeze-dried one but higher intensity due to its more compact and smoother structure. The CrI of air-dried F4 was calculated to be 80.8%, slightly higher than the 77.9% of its freeze-dried counterpart. It is interesting that the 80.8% of the air-dried F4 is close to the air-dried TEMPO oxidized CNFs

DOI: 10.1021/acssuschemeng.5b01653
ACS Sustainable Chem. Eng. 2016, 4, 1697−1706

(80%), although the freeze-dried one is significantly higher (77.9% for F4 vs 66.3% for TEMPO oxidized CNFs).[44] This result further corroborates the hypothesis that induced crystallization is expected to occur during ultrafiltration and air-drying, which seem to supersede the differences in nanocellulose types. Therefore, rapid freezing and freeze-drying of CNFs appear to preserve the crystal structures of nanocellulose and serve better in determining their crystallinity. In essence, air-drying induced crystallization and improved thermal stability regardless of the types of nanocellulose.

CONCLUSIONS

Rice straw cellulose was mechanically defibrillated via ACC by processing 0.8 wt % aqueous dispersion at 180 MPa in 30 passes, then differentially centrifuged into four increasing weight fractions of progressively thinner cellulose nanofibrils (CNFs): 6.9% 80−200 nm, 14.4% 20−80 nm, 20.3% 5−20 nm, and 58.4% less than 5 nm in thickness. With an energy input of 15 kWh/kg (MWh/t), rice straw cellulose was 100% defibrillated into ca. 4 to 200 nm thick CNFs. Over 93.1% CNFs were less than 80 nm thick, more than double the yields from wood pulp by other mechanical means but at only one-fourth to one-third of energy. Furthermore, the finest CNFs were averaged 3.7 nm thick and 5.5 nm wide, much narrower than those obtained from bamboo (20 nm), hardwood pulp (21 nm), microbial cellulose pellicle (33 nm), and microcrystalline cellulose (17 nm) from the same ACC treatment. The combined F3 and F4 CNFs accounted for 78.7% of ACC defibrillated rice straw cellulose, were less than 20 nm thick, and could self-assemble into continuous, uniformly sized (ϕ = 136 nm) fibers with slightly higher crystallinity (CrI = 78%) but unchanged crystallite size of 3.5 nm. The self-assembled fibers were thinner, more uniform, and more thermally stable (T_{max} = 345−364 °C) than those from chemically isolated nanocellulose (T_{max} 269 °C for TEMPO oxidized CNFs, 234 °C for CNCs in acid form) from the same rice straw cellulose. Ultrafiltration followed by air-drying of CNFs produced semitransparent and mechanically strong films with increased crystallinity and improved thermal stability than their freeze-dried counterparts.

AUTHOR INFORMATION

Corresponding Author

*Tel: +1 530 752 0843. Fax: +1 530 752 7584. E-mail: ylhsieh@ucdavis.edu.

Notes

The authors declare no competing financial interest.

ACKNOWLEDGMENTS

We appreciate the funding support from the California Rice Research Board (Project RU-9).

REFERENCES

(1) Sun, R. C.; Tomkinson, J.; Ma, P. L.; Liang, S. F. Comparative study of hemicelluloses from rice straw by alkali and hydrogen peroxide treatments. *Carbohydr. Polym.* **2000**, *42* (2), 111−122.

(2) Sun, R. C.; Tomkinson, J.; Mao, F. C.; Sun, X. F. Physicochemical characterization of lignins from rice straw by hydrogen peroxide treatment. *J. Appl. Polym. Sci.* **2001**, *79* (4), 719−732.

(3) Rodriguez, A.; Sanchez, R.; Requejo, A.; Ferrer, A. Feasibility of rice straw as a raw material for the production of soda cellulose pulp. *J. Cleaner Prod.* **2010**, *18* (10−11), 1084−1091.

(4) Hasanjanzadeh, H.; Hedjazi, S.; Ashori, A.; Mahdavi, S.; Yousefi, H. Effects of hemicellulose pre-extraction and cellulose nanofiber on the properties of rice straw pulp. *Int. J. Biol. Macromol.* **2014**, *68*, 198−204.

(5) Rodriguez, A.; Moral, A.; Serrano, L.; Labidi, J.; Jimenez, L. Rice straw pulp obtained by using various methods. *Bioresour. Technol.* **2008**, *99* (8), 2881−2886.

(6) Navaee-Ardeh, S.; Mohammadi-Rovshandeh, J.; Pourjoozi, M. Influence of rice straw cooking conditions in the soda-ethanol-water pulping on the mechanical properties of produced paper sheets. *Bioresour. Technol.* **2004**, *92* (1), 65−69.

(7) Chen, X. L.; Yu, J.; Zhang, Z. B.; Lu, C. H. Study on structure and thermal stability properties of cellulose fibers from rice straw. *Carbohydr. Polym.* **2011**, *85* (1), 245−250.

(8) Reddy, N.; Yang, Y. Q. Properties of high-quality long natural cellulose fibers from rice straw. *J. Agric. Food Chem.* **2006**, *54* (21), 8077−8081.

(9) El-Sakhawy, M.; Hassan, M. L. Physical and mechanical properties of microcrystalline cellulose prepared from agricultural residues. *Carbohydr. Polym.* **2007**, *67* (1), 1−10.

(10) Ibrahim, M. M.; El-Zawawy, W. K.; Juttke, Y.; Koschella, A.; Heinze, T. Cellulose and microcrystalline cellulose from rice straw and banana plant waste: preparation and characterization. *Cellulose* **2013**, *20* (5), 2403−2416.

(11) Somerville, C.; Bauer, S.; Brininstool, G.; Facette, M.; Hamann, T.; Milne, J.; Osborne, E.; Paredez, A.; Persson, S.; Raab, T.; Vorwerk, S.; Youngs, H. Toward a systems approach to understanding plant-cell walls. *Science* **2004**, *306* (5705), 2206−2211.

(12) Habibi, Y.; Lucia, L. A.; Rojas, O. J. Cellulose nanocrystals: chemistry, self-assembly, and applications. *Chem. Rev.* **2010**, *110* (6), 3479−3500.

(13) Abe, K.; Yano, H. Comparison of the characteristics of cellulose microfibril aggregates of wood, rice straw and potato tuber. *Cellulose* **2009**, *16* (6), 1017−1023.

(14) Hassan, M. L.; Fadel, S. M.; El-Wakil, N. A.; Oksman, K. Chitosan/rice straw nanofibers nanocomposites: Preparation, mechanical, and dynamic thermomechanical properties. *J. Appl. Polym. Sci.* **2012**, *125*, E216−E222.

(15) Nasri-Nasrabadi, B.; Behzad, T.; Bagheri, R. Extraction and characterization of rice straw cellulose nanofibers by an optimized chemomechanical method. *J. Appl. Polym. Sci.* **2014**, *131*, 40063−40070.

(16) Nasri-Nasrabadi, B.; Behzad, T.; Bagheri, R. Preparation and characterization of cellulose nanofiber reinforced thermoplastic starch composites. *Fibers Polym.* **2014**, *15* (2), 347−354.

(17) Jiang, F.; Hsieh, Y.-L. Chemically and mechanically isolated nanocellulose and their self-assembled structures. *Carbohydr. Polym.* **2013**, *95* (1), 32−40.

(18) Lu, P.; Hsieh, Y. L. Preparation and characterization of cellulose nanocrystals from rice straw. *Carbohydr. Polym.* **2012**, *87* (1), 564−573.

(19) Jiang, F.; Dallas, J. L.; Ahn, B. K.; Hsieh, Y. L. 1D and 2D NMR of nanocellulose in aqueous colloidal suspensions. *Carbohydr. Polym.* **2014**, *110*, 360−366.

(20) Hsieh, Y. L. Cellulose nanocrystals and self-assembled nanostructures from cotton, rice straw and grape skin: a source perspective. *J. Mater. Sci.* **2013**, *48* (22), 7837−7846.

(21) Jiang, F.; Han, S.; Hsieh, Y.-L. Controlled defibrillation of rice straw cellulose and self-assembly of cellulose nanofibrils into highly crystalline fibrous materials. *RSC Adv.* **2013**, *3* (30), 12366−12375.

(22) Gu, J.; Hsieh, Y.-L. Surface and Structure Characteristics, Self-Assembling, and Solvent Compatibility of Holocellulose Nanofibrils. *ACS Appl. Mater. Interfaces* **2015**, *7* (7), 4192−4201.

(23) Jiang, F.; Hsieh, Y.-L. Assembling and Redispersibility of Rice Straw Nanocellulose: Effect of tert-Butanol. *ACS Appl. Mater. Interfaces* **2014**, *6* (22), 20075−20084.

(24) Jiang, F.; Hsieh, Y. L. Amphiphilic superabsorbent cellulose nanofibril aerogels. *J. Mater. Chem. A* **2014**, *2* (18), 6337−6342.

DOI: 10.1021/acssuschemeng.5b01653
ACS Sustainable Chem. Eng. 2016, 4, 1697−1706

(25) Jiang, F.; Hsieh, Y.-L. Super water absorbing and shape memory nanocellulose aerogels from TEMPO-oxidized cellulose nanofibrils via cyclic freezing-thawing. *J. Mater. Chem. A* **2014**, *2* (2), 350−359.
(26) Kondo, T.; Morita, M.; Hayakawa, K.; Onda, Y. Wet Pulverizing of Polysaccharides. U.S. Patent 7,357,339, 2008.
(27) Kose, R.; Mitani, I.; Kasai, W.; Kondo, T. "Nanocellulose" as a single nanofiber prepared from pellicle secreted by gluconacetobacter xylinus using aqueous counter collision. *Biomacromolecules* **2011**, *12* (3), 716−720.
(28) Kondo, T.; Kose, R.; Naito, H.; Kasai, W. Aqueous counter collision using paired water jets as a novel means of preparing bio-nanofibers. *Carbohydr. Polym.* **2014**, *112*, 284−290.
(29) Wilson, K.; Walker, J. Centrifugation Techniques. In *Principles and Techniques of Practical Biochemistry*, 5th ed.; Cambridge University Press: Cambridge, U.K., 2000; pp 263−271.
(30) Jiang, F.; Esker, A. R.; Roman, M. Acid-catalyzed and solvolytic desulfation of H_2SO_4-hydrolyzed cellulose nanocrystals. *Langmuir* **2010**, *26* (23), 17919−17925.
(31) Segal, L.; Creely, J. J.; Martin, A. E., Jr.; Conrad, C. M. An empirical method for estimating the degree of crystallinity of native cellulose using the x-ray diffractometer. *Text. Res. J.* **1959**, *29*, 786−794.
(32) Scherrer, P. Estimation of the size and internal structure of colloidal particles by means of Röntgen rays. *Nachrichten von der Gesellschaft der Wissenschaften zu Göttingen* **1918**, 96−100.
(33) Wang, S.; Cheng, Q. A Novel Process to Isolate Fibrils from Cellulose Fibers by High-Intensity Ultrasonication, Part 1: Process Optimization. *J. Appl. Polym. Sci.* **2009**, *113* (2), 1270−1275.
(34) Wang, Q. Q.; Zhu, J. Y.; Gleisner, R.; Kuster, T. A.; Baxa, U.; McNeil, S. E. Morphological development of cellulose fibrils of a bleached eucalyptus pulp by mechanical fibrillation. *Cellulose* **2012**, *19* (5), 1631−1643.
(35) Taipale, T.; Osterberg, M.; Nykanen, A.; Ruokolainen, J.; Laine, J. Effect of microfibrillated cellulose and fines on the drainage of kraft pulp suspension and paper strength. *Cellulose* **2010**, *17* (5), 1005−1020.
(36) Tsuboi, K.; Yokota, S.; Kondo, T. Difference between bamboo- and wood-derived cellulose nanofibers prepared by the aqueous counter collision method. *Nord. Pulp Pap. Res. J.* **2014**, *29* (1), 069−076.
(37) Cheng, G.; Zhang, X.; Simmons, B.; Singh, S. Theory, practice and prospects of X- ray and neutron scattering for lignocellulosic biomass characterization: towards understanding biomass pretreatment. *Energy Environ. Sci.* **2015**, *8* (2), 436−455.
(38) Cheng, G.; Varanasi, P.; Li, C.; Liu, H.; Menichenko, Y. B.; Simmons, B. A.; Kent, M. S.; Singh, S. Transition of Cellulose Crystalline Structure and Surface Morphology of Biomass as a Function of Ionic Liquid Pretreatment and Its Relation to Enzymatic Hydrolysis. *Biomacromolecules* **2011**, *12* (4), 933−941.
(39) Fernandes, A. N.; Thomas, L. H.; Altaner, C. M.; Callow, P.; Forsyth, V. T.; Apperley, D. C.; Kennedy, C. J.; Jarvis, M. C. Nanostructure of cellulose microfibrils in spruce wood. *Proc. Natl. Acad. Sci. U. S. A.* **2011**, *108* (47), E1195−E1203.
(40) Wada, M.; Kondo, T.; Okano, T. Thermally induced crystal transformation from cellulose I-alpha to I-beta. *Polym. J.* **2003**, *35* (2), 155−159.
(41) Martinez-Sanz, M.; Lopez-Rubio, A.; Lagaron, J. M. Optimization of the nanofabrication by acid hydrolysis of bacterial cellulose nanowhiskers. *Carbohydr. Polym.* **2011**, *85* (1), 228−236.
(42) Kargarzadeh, H.; Ahmad, I.; Abdullah, I.; Dufresne, A.; Zainudin, S. Y.; Sheltami, R. M. Effects of hydrolysis conditions on the morphology, crystallinity, and thermal stability of cellulose nanocrystals extracted from kenaf bast fibers. *Cellulose* **2012**, *19* (3), 855−866.
(43) Roman, M.; Winter, W. T. Effect of sulfate groups from sulfuric acid hydrolysis on the thermal degradation behavior of bacterial cellulose. *Biomacromolecules* **2004**, *5* (5), 1671−1677.
(44) Jiang, F.; Hsieh, Y.-L. Self-assembling of TEMPO oxidized cellulose nanofibrils as effected by protonation of surface carboxyls and drying methods. *ACS Sustainable Chem. Eng.* **2016**, DOI: 10.1021/acssuschemeng.5b01123.
(45) Zhu, H.; Zhu, S.; Jia, Z.; Parvinian, S.; Li, Y.; Vaaland, O.; Hu, L.; Li, T. Anomalous scaling law of strength and toughness of cellulose nanopaper. *Proc. Natl. Acad. Sci. U. S. A.* **2015**, *112* (29), 8971−8976.
(46) Fukuzumi, H.; Saito, T.; Iwata, T.; Kumamoto, Y.; Isogai, A. Transparent and high gas barrier films of cellulose nanofibers prepared by TEMPO-mediated oxidation. *Biomacromolecules* **2009**, *10* (1), 162−165.
(47) Fukuzumi, H.; Saito, T.; Isogai, A. Influence of TEMPO-oxidized cellulose nanofibril length on film properties. *Carbohydr. Polym.* **2013**, *93* (1), 172−177.

DOI: 10.1021/acssuschemeng.5b01653
ACS Sustainable Chem. Eng. 2016, 4, 1697−1706